J. Fluid Mech. (1997), *vol.* 334, *pp.* 381–409

Mixing and reaction in curved liquid shear layers

By P. S. KARASSO AND M. G. MUNGAL

Thermosciences Division, Mechanical Engineering Department, Stanford University, Stanford CA 94305-3032, USA

(Received 21 September 1994 and in revised form 28 October 1996)

The concentration field of mixing layers subject to stabilizing and destabilizing streamwise curvature was investigated at post-mixing-transition conditions. A set of operating conditions was implemented, identical to those at which straight layers were previously investigated in the same facility, in order to compare the effects of hydrodynamic instabilities upon scalar mixing. Quantitative imaging of planar laser-induced fluorescence was used for (i) passive scalar measurements, and (ii) chemical product measurements. Similar to the straight mixing layer, the results for the curved layers show that beyond the mixing transition the layer continues to evolve, and undergoes a small change in its scalar structure. At conditions just past the mixing transition both stable and unstable layers have average mixed-fluid compositions which are uniform across the layer, and average chemical product concentration profiles which are symmetric. At more fully developed conditions, the scalar field evolved: the average mixed-fluid concentration developed a small lateral variation, while the chemical product concentration profiles became asymmetric. Similar to the straight layer, the mixture-fraction PDF is believed to be of the tilted type for the most fully developed layer examined, with the marching PDF being a poor representation. Consistent with previous investigations, the growth rate of the unstable layer was found to be higher than that of straight or stable layers. The most important result is that the measured mixing efficiency of all the layers (curved and straight) was found to be the same: both the total mixed-fluid composition, and the volume fraction of mixed fluid were the same for all unstable, stable, and straight layers. The amount of mixed fluid (and of chemical product formed) was larger for the unstable layer, but always in a fixed proportion to the layer's thickness. The lack of increase in the mixing efficiency for the unstable layer is surprising, given that previous hydrodynamic measurements had shown enhanced turbulent transport for the unstable case. Thus, for all liquid shear layers studied, the rate of scalar mixing appears to be directly proportional to the entrainment rate (which essentially determines the layer's growth rate), and not to any hydrodynamic measures.

1. Introduction

Many issues regarding turbulent mixing pose significant challenges to those who seek to model or calculate the governing physical phenomena. Experiments are needed to guide mixing models. In a companion paper (Karasso & Mungal 1996, referred to herein as K&M), we presented the results of a set of experiments to measure the composition and the amount of molecularly mixed fluid across the plane mixing layer. The study was performed at increasing Reynolds numbers, and with different initial and operating conditions, in order to quantify how the various parameters affect scalar mixing. The plane (straight) shear layer was chosen as a model flow with relatively simple boundary conditions and strong similarity properties.

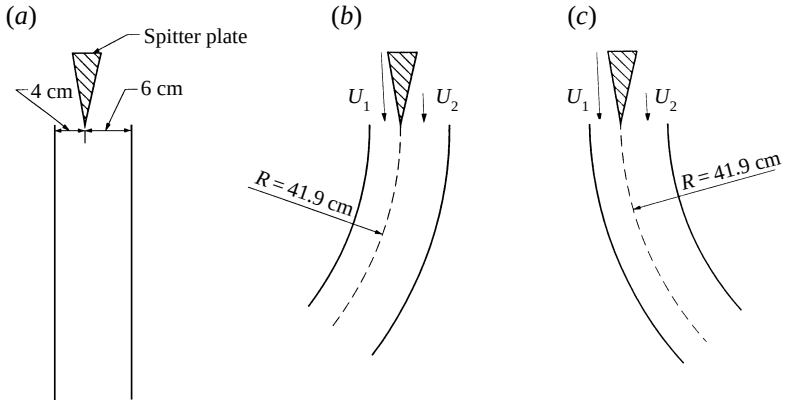

FIGURE 1. Schematic for (*a*) straight, (*b*) unstable and (*c*) stable shear-layer geometries. The high-speed fluid stream is 4 cm in height, the low-speed stream is 6 cm in height. The span is 16 cm into paper.

Following that work, we now study mixing in a flow with one additional degree of complexity, in an effort to supplement and systematically build on the existing knowledge of turbulent mixing. This additional degree of complexity is curvature, which is also naturally present in many practical flows. Shear layers which are curved in the longitudinal direction are characterized as stable and unstable: unstable when the faster fluid is placed on the inside of the bend (figure 1*b*), and stable in the opposite case (figure 1*c*). The sense of curvature is important since a number of studies have shown that even mild curvature produces significant changes (with respect to the straight mixing layer, figure 1*a*) in the growth rate, the turbulent (hydrodynamic) transport properties, and the three-dimensionality of the layer.

In a curved shear layer, the inflectional Kelvin–Helmholtz (K–H) instability is present when $U_1 \neq U_2$ (where U is the free-stream velocity magnitude, and subscripts 1 and 2 denote the high- and the low-speed streams respectively). Additionally, curvature introduces centrifugal forces which tend to produce streamwise vortical structures of the Taylor–Görtler type. Rayleigh (1880) showed that the stability condition for an inviscid flow depends on the sign (positive or negative) of the radial gradient of angular momentum. Synge (1933) gave the stability criterion in the form $(\mathrm{d}/\mathrm{d}r)(\rho U^2 r^2) > 0$; thus, for layers of uniform density ($\rho_1 = \rho_2$), the layer is stable when $U_{outer} > U_{inner}$, and unstable when $U_{inner} > U_{outer}$. Also, note that a density difference may also produce an unstable layer (Wang 1984); the associated instability mechanism is known as the Rayleigh–Taylor instability.

Extensive hydrodynamic (velocity) measurements in a single-stream curved shear layer were performed by Margolis & Lumley (1965) and Wyngaard *et al.* (1968), for both stable and unstable configurations. They found that the shear stresses are higher for the unstable layer: both the peak and the width of the shear stress distribution were enhanced. Gibson & Younis (1983) studied a single-stream mildly curved unstable layer: they measured enhanced growth rates and shear stresses, compared to the respective values for a straight shear layer.

The degree of curvature is often measured through the flux Richardson number, $R_f = 2S/(1+2S)$, where $S = (\partial V/\partial x)/(\partial U/\partial y)$. The choice of this parameter is arbitrary, but it provides a way for accounting for the extra rates of strain that curvature introduces in a turbulent field. Another parameter used to describe the strength of curvature is δ/R, where δ is the local thickness of the layer, and R is the

radius of the curvature imposed. Bradshaw (1973) has reviewed the effects of streamline curvature on turbulent flows, and discusses various issues and dimensionless parameters pertaining to curved mixing layers. In our study, the layers have $\delta/R \leqslant 0.15$, which is considered to be 'mild' curvature.

Following the suggestion of G. L. Brown, Wang (1984) was the first investigator to perform flow visualizations (schlieren) in stable and unstable shear layers, at various speed ratios and density ratios. Wang worked in the spirit of providing evidence of the competition among the main instability mechanisms in a curved shear flow (Kelvin–Helmholtz, Taylor–Görtler, Rayleigh–Taylor). For the equal-density layers, he found that the sense of curvature had a large effect on the structure of the layer, and attributed this to the role of the Taylor–Görtler instability. For the unstable case, he noticed: (i) enhanced three-dimensionality with loss of the Kelvin–Helmholz structures, (ii) side views which showed multiple braids, interpreted as Taylor–Görtler rollers, (iii) increased growth rates compared to the stable cases (about 15% at a velocity ratio $U_1/U_2 = 2.6$), and (iv) inhibited pairings. Stable layers showed well-defined Kelvin–Helmholtz rollers. Wang also suggested that the height of the channel for curved layers might be an important scaling parameter, which could complicate the comparison of results from different facilities.

Plesniak & Johnston (1989), in a water shear-layer facility (modelled after Wang's facility), performed velocity measurements in plane, unstable, and stable configurations. Their results showed enhanced turbulent properties for the unstable layer (compared to stable and straight layers at the same operating conditions); all layers were characterized by three-dimensionality. The U-velocity component showed much greater spanwise variation for the unstable case, evidence of enhanced streamwise vorticity. Their measurements showed that self-similarity tends to be achieved sooner (in downstream distance) for the unstable and the straight layer, while the stable layer was the least fully developed. At the furthest downstream measuring point ($Re \approx 14000$), they found the peak of the Reynolds normal stress for the unstable layer to be $\sim 30\%$ larger than for the straight layer, and $\sim 100\%$ larger than for the stable layer. Interestingly, the Reynolds shear stresses at that station were identical for all three layers. The unstable layer was more intermittent, and had enhanced turbulent transport (with the straight following, and the stable being last). A more recent study by Plesniak, Mehta & Johnston (1994), showed well-defined spatially stationary streamwise vorticity to exist in both stable and unstable layers developing from untripped initial boundary layers. The source of this vorticity, however, appeared to be the amplification of small incoming disturbances (similar to that in straight layers), rather than the Taylor–Görtler instability. When the initial boundary layer was tripped, no coherent streamwise vorticity was found in either stable or unstable configurations.

A numerical hydrodynamic stability analysis of curved shear flows was recently performed by Liou (1993). For stable curved layers, the Kelvin–Helmholtz modes showed reduced growth rates. For unstable layers, he predicted counter-rotating streamwise vortex pairs and more unstable K–H modes. Additional strong modes were also found for the unstable case.

Scalar mixing

To date, except for the few average-concentration profiles shown in Wang's thesis, no quantitative scalar mixing measurements exist for curved shear layers. It would be interesting to know whether the observed hydrodynamic changes in curved layers are also accompanied by a change in the scalar field. Some important questions are: (i) Does the observed increase in the growth rate of the unstable layer translate into an

increase in the total amount of mixed fluid, i.e. does increased stirring lead to an increased amount of mixing? (ii) Does the mixing efficiency (defined by the probability of mixed fluid) increase, suggesting that the enhancement of turbulent transport leads to better fine-scale molecular mixing, i.e. does increased stirring lead to increased mixing efficiency? In the context of technological applications, mixing enhancement could be achieved by imposing mild curvature in the flow field. The economy of such a configuration might come from a relatively simple implementation, with only small penalties in pressure drop. Furthermore, from a flow physics point of view, it is important to understand the effects of the interaction between the streamwise and the spanwise vortices on the structure of the mixing layer.

The present paper supposes familiarity with our previous work on straight mixing layers (K & M). Here our purpose is to examine the scalar structure of curved mixing layers at various operating conditions, and compare it to that of straight layers. We examine stable and unstable layers at conditions identical to those at which straight layers were examined. The planar laser induced fluorescence (PLIF) technique is used for both chemical product and passive scalar measurements, and the goal is to measure the distribution and composition of mixed fluid, the growth rate of the layer, and the occurrence (or lack of) of large-scale structures. Complete details of all aspects of this work can be found in Karasso (1994).

2. Experimental details

This section gives only a very brief description of the experiments, and the reader should consult K & M for further details.

2.1. *Facility*

The facility consists of a blow-down water tunnel with two independent feeding plenums for the two streams of the mixing layer. The velocity magnitudes of the two streams are controlled independently, thus the facility can be operated at various speed ratios. The design of the test section is modular, so that curved or straight guide walls can be mounted, figure 1. For the study of curved layers, a different set of walls was machined for each case (unstable, stable). Both stable and unstable test sections were designed to have the same mean radius of curvature ($R_{mean} \approx 41.9$ cm). The curved walls have a length corresponding to a circular arc section of 40° for the unstable, and 45° for the stable case. The test section consists of straight endwalls and has a size of 16 cm (span), by 10 cm (height of channel) consisting of 4 cm allocated to the high-speed flow and 6 cm to the low-speed flow. We denote by s the streamwise direction (along an arc of constant radius), y the cross-stream direction (layer thickness), and z the spanwise direction.

2.2. *PLIF technique*

Planar laser-induced fluorescence (PLIF) was used to acquire quantitative images of the concentration field across the layer. All the details of the imaging technique, the PLIF-signal calibrations, and the data reduction are given in K & M. For all experiments in the present work we used the copper-vapour laser (at the 510.6 nm line) with sodium fluorescein as the fluorescent tracer. The laser beam was formed into a sheet of light, and a 2D CCD array (Cohu 6510) was used to acquire images of the flow field at a right angle to the light sheet.

The PLIF method was used for two types of measurements: (*a*) passive scalar measurements, and (*b*) chemical product measurements. In the passive scalar

measurements the dye is uniformly seeded into one of the feeding reservoirs (usually the low-speed one), while the other reservoir contains pure water. The acquired signals represent the local mixture fraction, i.e. the volume fraction of high-speed fluid in the mixture. Due to resolution inadequacies, the passive scalar method is known to yield erroneous results: in fact, we explicitly showed in our previous study the significant errors of the passive scalar method. Therefore, in the present work more emphasis will be placed on the chemical-reaction data. The previous work however established that passive scalar PDFs reflect changes in the flow that are seen in the chemical reaction measurements, and as such serve as a diagnostic of changes in the scalar field; it is in this spirit that the passive scalar results are presented.

The implementation of the chemical-reaction method involves a fast reaction of the type $A + B \rightarrow P$, where reactant A (H_2SO_4 acid solution, pH $\approx$ 3) is diluted into one free stream, and reactant B (NaOH base solution, pH $\approx$ 12.3) into the other free stream. The acid base reaction between the two free-stream fluids is used to 'turn on' the fluorescence of a pH-sensitive dye (sodium fluorescein), which is diluted uniformly in the reservoir with the acidic solution. The imaged fluorescence represents the product P, and each image provides an instantaneous spatial distribution of chemical-product concentration across the layer.

The stoichiometric ratio of the acid base reaction, ϕ, is defined as the volume parts of high-speed fluid needed to titrate (i.e. raise the pH to a level where the dye fluorescence is 'turned on') one part of low-speed fluid. As explained in K & M, a pair of 'flip experiments' was run for each case layer, where the same reactants were exchanged between the high- and the low-speed side. Thus, each layer case was measured both at $\phi = \frac{16}{1}$ and $\phi = \frac{1}{16}$. These two runs are taken as representative of runs with $\phi \rightarrow \infty$ ('very high' ϕ) and $\phi \rightarrow 0$ ('very low' ϕ). As shown by Koochesfahani & Dimotakis (1986), each pair of flip runs (providing information on the chemical-product concentration) is the basis for making resolution-free estimates of *mixed-fluid* quantities (i.e. average mixture fraction).

2.3. *Experimental conditions*

Table 1 summarizes the operating conditions for the unstable and the stable configurations. A first set of experiments was performed at a speed ratio $r = U_2/U_1 = \frac{1}{4}$: three different cases were examined, corresponding to high-speed-stream velocity magnitude (U_1) of 0.34, 0.95 and 1.90 m s^{-1} respectively. A second set of experiments was performed at a speed ratio $r = 1/2.65$, at $U_1 = 0.70$ and 1.05 m s^{-1}. For each case, the (laminar) boundary-layer momentum thickness, θ, at the tip of the splitter plate, was estimated using Thwaites method (table 1). For a few cases, a trip wire (1.6 mm in diameter, positioned at 6 cm upstream of the splitter-plate tip) was placed on the splitter plate at the high-speed side, in order to cause the boundary layer to become turbulent. The cases where the trip wire was used will be termed 'tripped', and the others 'untripped'. The passive scalar method was used to measure the layers (unstable and stable) at both $r = \frac{1}{4}$ and 1/2.65. Chemical-reaction experiments were only performed for the $r = \frac{1}{4}$ cases. Notice that, for the same operating conditions, the thickness of the stable and unstable layers is different and so the assigned Reynolds number (*Re*) will be different (and will also be different from the *Re* of straight layers at identical conditions). In this work, *Re* is defined by the free-stream velocity difference, the 1% thickness of the layer (which is essentially the same as the visual thickness of the layer) and the kinematic viscosity of water.

One of the major conclusions of K & M was that the Reynolds number alone is inadequate to characterize the mixing layer. The 'pairing parameter', Rx/λ (where $R =$

Speed ratio	U_1 (m s^{-1})	Initial b.l.	δ (cm) at $x = 23$ cm	Re	L/λ_B	$Rs/30\theta$	PDF type
			Unstable layer				
1/4	0.34	Untripped	5.20	13600	800	16.3	Dual
1/4	0.95	Untripped	4.81	35000	1740	27	Marching
1/4	1.9	Untripped	4.47	65000	2980	38.3	Marching
1/2.63	0.7	Untripped	3.92	17400	1260	17.2	Dual
1/2.63	0.7	Tripped	3.42	15100	1300	—	Marching
1/2.63	1.05	Untripped	3.36	22300	1780	21.6	Marching
			Stable layer				
1/4	0.34	Untripped	5.21	13600	800	17.8	Non-marching
1/4	0.95	Untripped	4.65	33800	1750	29.5	Dual
1/4	1.9	Untripped	4.34	63100	3000	42	Dual
1/2.63	0.7	Untripped	4.25	18800	1230	18.7	Dual
1/2.63	0.7	Tripped	3.29	14600	1320	—	Marching
1/2.63	1.05	Untripped	3.34	22200	1780	23.5	Marching

TABLE 1. Operating conditions, and summary of passive-scalar results for curved layers.

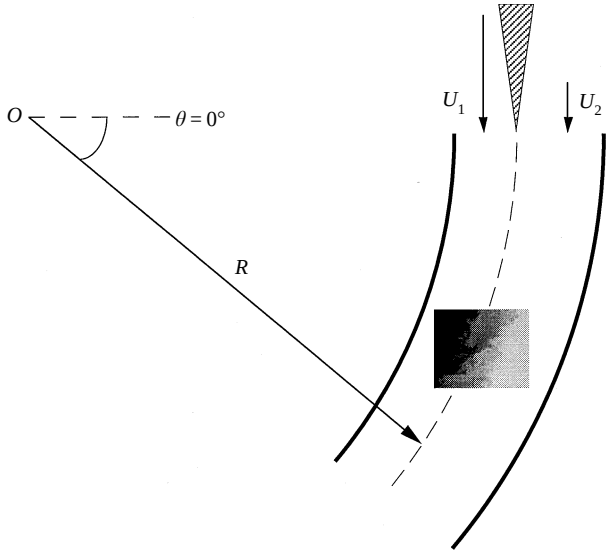

FIGURE 2. Image of an unstable layer, placed schematically with respect to the test section.

$(1-r)/(1+r)$, x is the downstream distance, and $\lambda \approx 30\theta$ is the most unstable wavelength), introduced by Huang & Ho (1990) (see also Jimenez 1983), which incorporates initial-condition effects and scales with the number of pairings in the mixing layer, was found adequate to show the differences in the shape of the PDF of the straight layer, and to give consistent trends for the measured product thickness. It is thus logical to expect that the Reynolds number may again be inadequate in characterizing curved layers. Thus, an equivalent pairing parameter, Rs/λ, will be used to 'label' each curved case (where s is now the streamwise distance at which the measurements are taken). When hydrodynamic measurements of the Huang & Ho (1990) type become available for curved layers, it may prove possible to relate the parameter Rs/λ to the number of pairings (or other phenomena) that occur in the

curved geometries. For the purposes of this study, it is important to keep in mind that the curved layers are examined at conditions identical to the conditions at which straight layers were measured, and the focus here is to compare between curved (stable and unstable) and straight layers, rather than to assign Rs/λ an absolute meaning.

Finally, an important issue regarding data reduction is the coordinate system of the curved layers. Figure 2 shows a measured (passive scalar) side-view image of an unstable layer placed schematically relative to the test section. It is seen that the flow's streamwise direction is now a path along a section of constant radius, whereas the cross-stream direction at a given point in the layer is now along a ray (constant angle θ) which emanates from the centre of curvature (point O in figure 2). The thickness, δ, of the layer was obtained along lines of constant θ, by averaging all images for each case. Also, to keep the notation simple, we shall denote as y/δ the normalized position across the curved layer, where y is now in the direction of R.

3. Passive scalar results

3.1. *Panoramic side views*

Panoramic (qualitative) side views were obtained to provide insight into the structure of the layer, and to yield growth rates. For both unstable and stable layers, the panoramic views were obtained for the three $r = \frac{1}{4}$ cases at $U_1 = 0.34$, 0.95 and 1.90 m s^{-1}. A sample of images is shown in figure 3 (unstable), and in figure 4 (stable). The white band that appears at the right-hand side in the stable-layer views is due to image processing difficulties resulting from the lack of a well-defined free stream in that region. The magnification ratio of the camera was about 0.043. In these images, flow is from left to right, and the high-speed stream is at the bottom of each image. All images were obtained with the passive scalar method, with dye seeded uniformly into the low-speed reservoir; however, the signals were remapped to make both sides appear dark (in the unprocessed images the low-speed side is bright). Parts of the side test-section walls are shown in each image, to aid the reader in following the flow. The views show the existence of K–H rollers for all cases; the K–H structures are especially well-defined for the lowest velocity case ($U_1 = 0.34$ m s^{-1}). For each case, the individual realizations showed evidence of both quasi-two-dimensional organized motion, as well as three-dimensionality. In order to determine the rate of occurrence of organized structures in the flow, the individual images in the region $x = 14$–28 cm were examined (about 35 images for each case). Images clearly displaying coherent K–H rollers (e.g. figure 3*a*, *c*) were taken as 'organized motion', whereas images with a three-dimensional appearance (e.g. figure 3*b*) as well as images that appeared ambiguous (figure 4*c*), were taken as 'no organization'. The results are given in table 2, with each case quoted as $Re\,(\mathrm{cm}^{-1}) = (U_1 - U_2)/\nu$. The results for the straight layer, as taken from K & M, are also included in this table.

It is seen that the unstable layers show consistently a slightly diminished rate of occurrence of well-defined structures with respect to the stable cases. Also, the values for the stable layer are almost identical to the values quoted for the straight layers.

The panoramic views for each case were averaged to extract information on the average growth rate of the layer. The spreading rate was obtained from the layers' edges, at locations where the local Reynolds number was larger than 12000 (we are interested in the far field), and was fitted to the formula

$$\frac{\delta}{s} = C_\delta \frac{1-r}{1+r}.$$

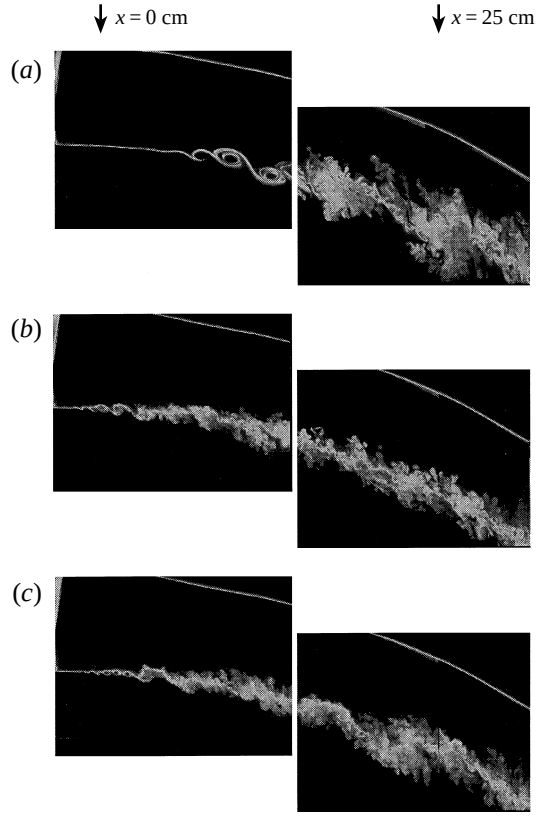

FIGURE 3. Panoramic side views for the unstable layer (each composed of two independent images). (*a*) $r = \frac{1}{4}$, $U_1 = 0.34$ m s^{-1}; (*b*) $r = \frac{1}{4}$, $U_1 = 0.95$ m s^{-1}; (*c*) $r = \frac{1}{4}$, $U_1 = 1.90$ m s^{-1}.

The resulting C_δ appear in table 2. The growth rates of the unstable layers are seen to be larger than those of stable layers by 4% to 14%. The smaller value pertains to the least developed case ($U_1 = 0.34$ m s^{-1}, $Re\,(\mathrm{cm}^{-1}) = 2600$), as inferred from points in the layer where the local Re was in the range of 13000 to 15000. The higher growth rates for the other two cases ($U_1 = 0.95$ and 1.90 m s^{-1}) were obtained from locations where the local Re was in the range of 30000 to 70000, and so they are more likely to represent the growth rate in the far field. The results are consistent with the findings of Wang (1984), who showed that the enhancement in the growth rate of unstable layers (compared to stable) continuously changes with downstream distance (or with increasing Re). For the far field, he found a 13% higher growth rate for the unstable layer. The results for C_δ, based on the thickness δ from the quantitative close-up visualizations (presented in the next section), are plotted in figure 5 for all curved cases (filled symbols represent tripped layers); the same plot includes the straight-layer results. The stable layers are seen to have growth rates just slightly smaller than the straight layers. Finally, as was found for the straight layer, the growth rate of curved layers decreases when the free-stream velocity magnitudes are increased.

Based on figures 3 and 4, and on the averaged panoramic views (not presented), it is seen that the layer has an initial no-growth region which extends to a distance s_0 downstream of the splitter-plate tip; the estimated s_0 for each case is given in table 2. For both curvatures, s_0 decreases as the velocity magnitudes are increased. Recall that in straight mixing layers, the initial no-growth region was also decreased when the layer

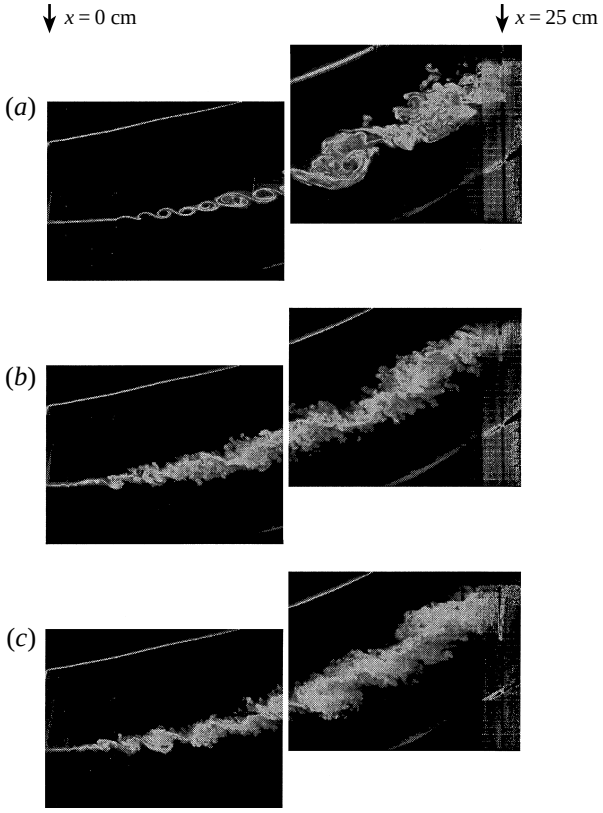

FIGURE 4. As figure 3 but for the stable layer.

Re (cm^{-1})	Organized motion (%)	No organization (%)	s_0 (cm)	C_δ
2600 unstable	69	31	3.8	0.38
2600 stable	75	25	5	0.37
2600 straight	72	28	—	0.36
7300 unstable	50	50	1.3	0.35
7300 stable	52	48	1	0.31
7300 straight	54	46	—	0.32
14500 unstable	48	52	1.3	0.34
14500 stable	52	48	1	0.29
14500 straight	52	48	—	0.30

TABLE 2. Statistics on the occurrence of coherent structures, growth rates for curved layers ($r = \frac{1}{4}$) and comparison with straight layers

was tripped (and tripping is believed to bring the layer closer to its asymptotic state at a shorter downstream distance (Bell & Mehta 1990)).

3.2. *Quantitative images*

Quantitative side-view images were obtained at magnification ratios $m \approx 0.071$ and $m \approx 0.076$ for the unstable and the stable configurations respectively. The camera was positioned so that the centre of the field of view was at downstream distances $s = 23$ cm

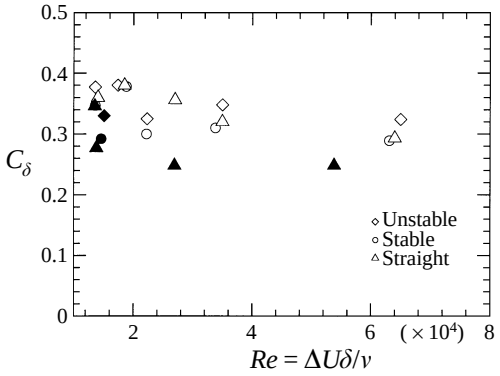

FIGURE 5. Spreading rate C_δ vs. Reynolds number, for straight, stable, and unstable layers (filled symbols represent tripped layers).

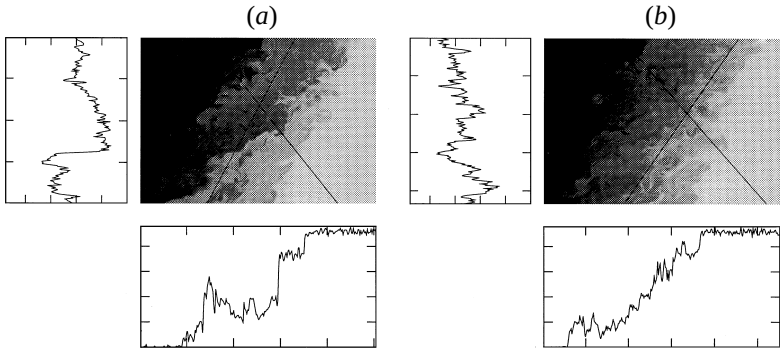

FIGURE 6. Passive scalar side views for the unstable $r = \frac{1}{4}$, $U_1 = 0.95$ m s^{-1} layer. Flow is from top to bottom. For each image, intensity profiles are shown for a streamwise cut (left), and a cross-stream cut (bottom).

and $s = 25$ cm (along the mean radius $R = 41.9$ cm, see figure 1), for the unstable and the stable cases respectively. The operating conditions are given in table 1. For each case, about 100 images were acquired to extract statistics.

The thickness (δ) for each layer was obtained by averaging the acquired images; it corresponds to the downstream position, s, at the centre of the imaged area. This thickness was used to calculate the Reynolds number (table 1); the estimated $Rs/30\theta$ for every case also appears in table 1.

A few typical images, corrected for laser beam non-uniformity and attenuation, are shown in figure 6. The flow direction is from top to bottom and tilted (since the test section is curved); the low-speed side was uniformly seeded with dye, and thus appears as the bright area on the right side of each image. Intensity profiles are shown for 'cuts' in the (nearly) streamwise and in the cross-stream directions. For each image, the streamwise profile is shown on the plot to the left, whereas the cross-stream cut is shown below. In K & M we showed how passive scalar measurements with inadequate spatial resolution are unreliable for predicting mixing quantities. For each of the curved layers, the measurements' relative resolution, L/λ_B, was calculated and is given in table 1. Here $L \approx 750$ μm is the light-sheet thickness (it is a measure of the sampling volume), and λ_B is the estimated Batchelor scale for each case. These numbers show that the imaging technique does not resolve the flow field. Hence, the present passive

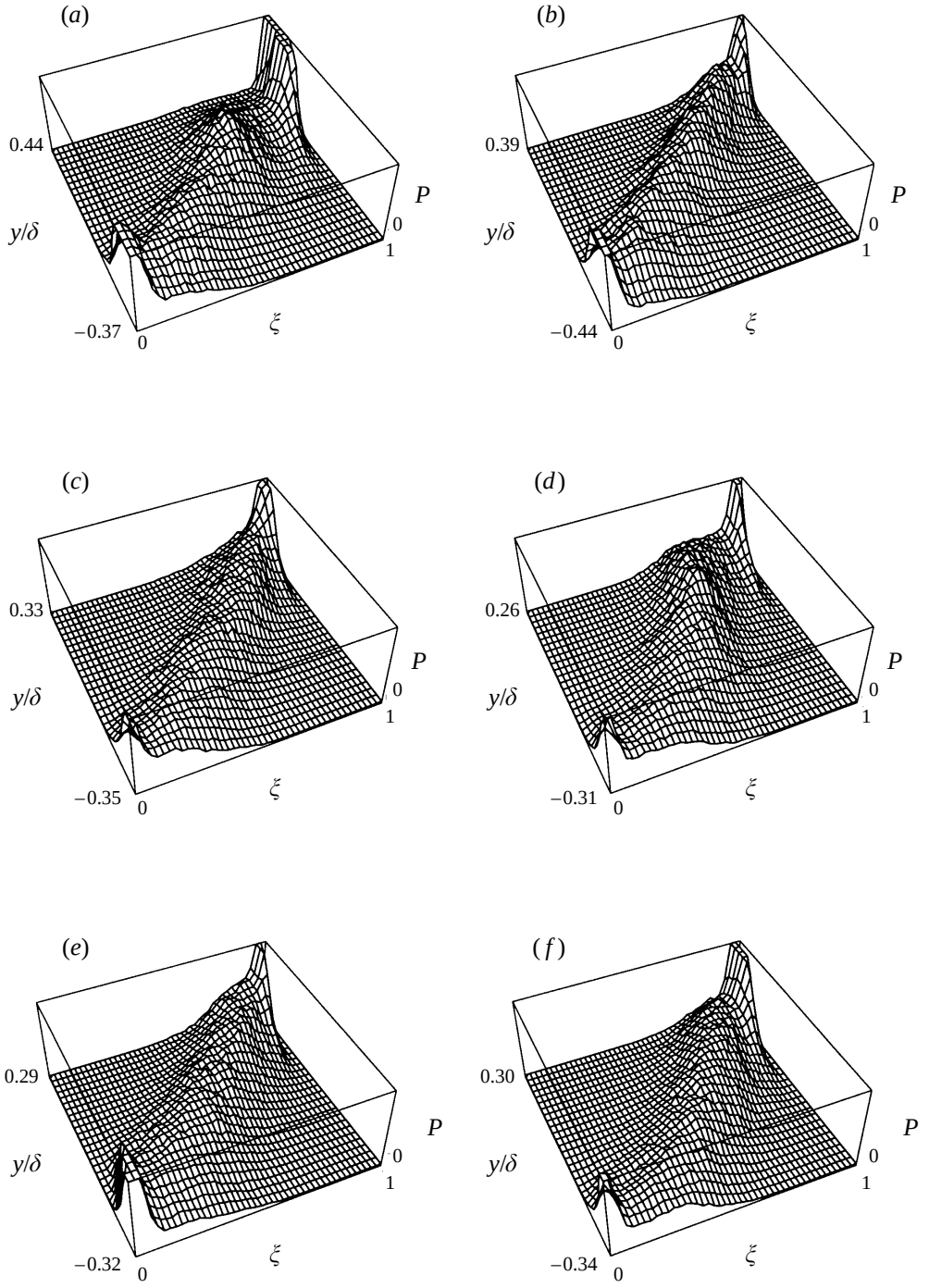

FIGURE 7. Passive scalar PDFs for the unstable layer. (*a*) $Re = 13600$ ($Rs/\lambda = 16.3$), (*b*) $Re = 35000$ ($Rs/\lambda = 27$), (*c*) $Re = 65000$ ($Rs/\lambda = 38.3$), (*d*) $Re = 17400$ ($Rs/\lambda = 17.2$), (*e*) $Re = 15100$ tripped. (*f*) $Re = 22300$ ($Rs/\lambda = 21.6$).

scalar results are expected to be in error. However, as was shown in K & M, the resolution discrepancy is believed to affect all cases in a similar way, and so comparison among the various cases can yield valid trends.

A common feature that we observed for all cases is the image-to-image variation, and the broad range of mixture fraction values across the layer. Consider the image of figure 6(*a*) for the $r = 1/4$, $U_1 = 0.95$ m s^{-1} unstable layer: both the streamwise and the cross-stream cuts show two structures with different intensity levels, but with each structure showing a preferred mixture-fraction value. In contrast, the image in figure 6(*b*) for the same case shows a ramped behaviour in both cuts. Resolution cannot be the only reason for this variety in the character of the layer, as we are comparing images of the same case (same relative resolution).

3.3. *The PDF*

Using the (processed) images, the probability density function (PDF) of the mixture fraction was extracted for each of the curved layers examined. The mixture fraction, ξ, is defined as the volume fraction of high-speed fluid into the mixture. Thus, $\xi = 0$ denotes pure low-speed fluid within the sampled volume, and $\xi = 1$ denotes pure high-speed fluid. The PDF of the mixture fraction, at a given location y across the layer, is given by

$$\mathrm{PDF}\,(\xi, y)\,\mathrm{d}\xi = \mathrm{Probability}\,\{\xi \leqslant \xi(y) \leqslant \xi + \Delta\xi\}.$$

Details on the definition of all statistical quantities used in this work can be found in K & M.

The PDFs are presented in figure 7 for the unstable layer, and in figure 8 for the stable layer. It is very important to remind the reader that, following the detailed discussion in K & M, the terms 'marching' and 'non-marching' are only used descriptively to label the different flow regimes in the layer, and not as defining the shape of the actual PDF. In K & M it was seen that changes in the PDF corresponded to fine-scale changes in the scalar mixing field which manifest themselves in the chemical reaction results; the passive scalar PDFs tend to overemphasize these changes but still serve as a diagnostic of changes occurring in the flow at sub-pixel dimensions whereby a 'non-marching' shape of the PDF is associated with a flow regime just past the mixing transition (less developed layer), and a 'marching' PDF reflects more fully developed conditions, after the occurrence of multiple vortex pairings. Again, the shape of the PDF is used here as a qualitative descriptor of the degree of development of the layer: the actual PDF shape cannot be determined, since passive scalar measurements (of inadequate resolution) are erroneous.

For the unstable case, the least developed layer $Rs/30\theta = 16.4$ ($Re = 13\,600$; $r = \frac{1}{4}$, $U_1 = 0.34$ m s^{-1}, figure 7*a*) shows a PDF which has a non-marching feature closer to the high-speed side, with marching behaviour towards the low-speed side. The non-marching part has a preferred mixture fraction value of about 0.68. Now, when the unstable layer (at the same speed ratio) is pushed to more fully developed conditions of $Rs/30\theta = 27$ ($Re = 35\,000$), and $Rs/30\theta = 38.3$ ($Re = 65\,000$), the PDF becomes marching (figure 7b, c). For the cases at the speed ratio of $r = 1/2.63$, the layer again has a behaviour similar to that of the straight layers: the least developed case $Rs/30\theta = 17.2$ ($Re = 17\,400$) shows a combination of marching and non-marching behaviour (figure 7*d*), and upon tripping the PDF turns into a marching one (figure 7*e*), suggesting that tripped layers reach a fully developed state earlier than untripped layers. When the free-stream velocity magnitudes are increased, a marching-type PDF is obtained for the $Rs/30\theta = 21.6$ ($Re = 22\,300$) layer (figure 7*f*), a behaviour similar to the $r = \frac{1}{4}$ cases.

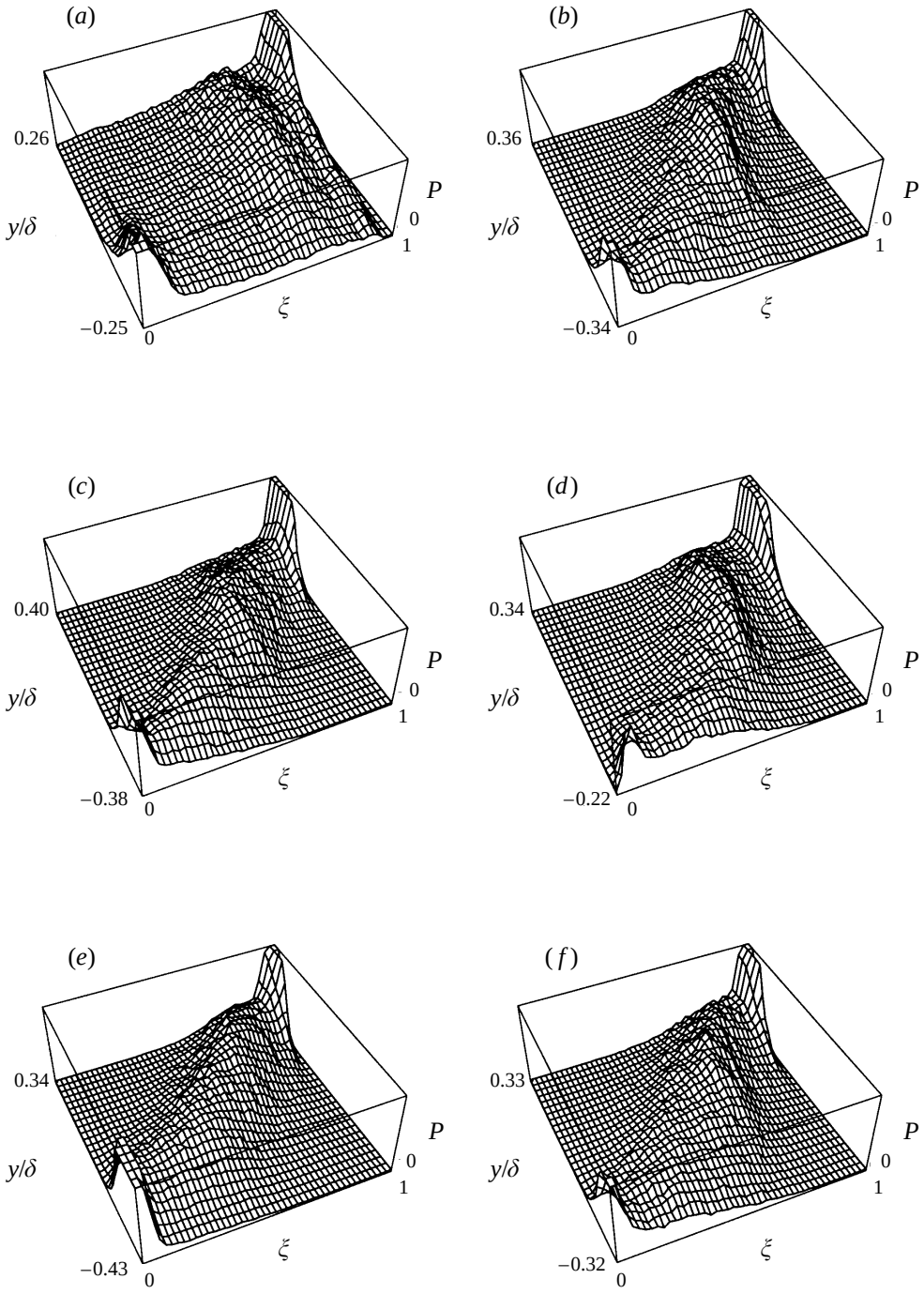

FIGURE 8. Passive scalar PDFs for the stable layer. (*a*) $Re = 13\,600$ ($Rs/\lambda = 17.8$), (*b*) $Re = 33\,800$ ($Rs/\lambda = 29.5$, (*c*) $Re = 63\,100$ ($Rs/\lambda = 42$), (*d*) $Re = 18\,800$ ($Rs/\lambda\,18.7$), (*e*) $Re = 14\,600$ tripped, (*f*) $Re = 22\,200$ ($Rs/\lambda = 23.5$).

For the stable layers we observe the following. For the least developed case $Rs/30\theta = 17.8$ ($Re = 13\,600$), the PDF is non-marching across the entire width of the layer (figure 8*a*). Comparing it with its unstable counterpart, it is evident that the stable layer is less developed at identical operating conditions. When the free-stream velocities are increased ($Rs/30\theta = 29.5$ and 42, for $U_1 = 0.95$ and 1.90 m s^{-1} respectively), the PDF develops a dual marching/non-marching behaviour (figure 8*b*, *c*). The stable layer behaves quite differently from the straight and the unstable layers: in those cases, the PDF shape was drastically changed when going from $U_1 = 0.35$ to 0.95 m s^{-1}. Furthermore, the stable layer at $Rs/\lambda = 42$ ($U_1 = 0.95$ m s^{-1}) is still not fully marching (figure 8*c*), but has the dual shape. These PDFs suggest that the stable layer has not yet reached the fully developed state of the previous layers at identical operating conditions. For the $r = 1/2.65$ cases, it is seen that tripping again alters the shape of the PDF (compare figure 8*d* to 8*e*), and drives the layer to a more developed regime.

3.4. *Summary of passive scalar results*

The passive scalar results presented here show that stable and unstable layers, like straight layers, can be characterized by both well-defined K–H-type rollers and a three-dimensional appearance. Stable layers tend to show more organization than unstable layers, and the statistics on the occurrence of organized motion (table 2) are similar to those of the straight case. In terms of growth rates, the unstable layer shows, at far-field conditions which are well beyond the mixing transition, an approximately 13% increase over its stable and straight counterparts. It is interesting to notice that in the least developed case ($r = \frac{1}{4}$, $U_1 = 0.34$ m s^{-1}), stable and unstable layers exhibit a smaller difference in growth rate within the measured region of the layer, i.e. for $Rs/\lambda < 20$ (or at the speed ratio of $\frac{1}{4}$, for $Re \leqslant 15000$). This is probably due to the fact that at these conditions, both layers are still in their early state of development, and have not yet reached the more fully developed state of the other two cases ($U_1 = 0.95$ and 1.90 m s^{-1}). This result is consistent with the findings of Wang (1984).

The passive scalar PDFs suggest that, for identical operating conditions, unstable layers are more fully developed than straight ones, while stable layers are less developed than their straight counterpart. The conclusion is based on the shapes of the PDFs obtained for the various cases, where it is assumed that non-marching behaviour is suggestive of less developed conditions, whereas marching behaviour suggests conditions closer to the asymptotic mixing state. Note that, given the poor resolution, these conclusions are not definitive; however, the straight-layer results in K & M have demonstrated that a shift in the shape of the measured passive scalar PDF was always accompanied by true changes in the flow structure, as revealed by the chemical data. It is thus essential to turn now to chemically reacting experiments in curved layers.

4. Chemical reaction experiments

The chemical reaction technique was used to measure the distribution of chemical product formed in the curved layers. For each case examined, a pair of flip experiments was performed at $\phi = 16$, and at $\phi = 1/16$. The reason why every case layer is measured at two different stoichiometries is that each pair of these chemical-product measurements allows us to estimate mixed-fluid quantities. These estimates are considered to be resolution-free, as the chemical-reaction method gives, on average, results which are not impeded by spatial resolution limitations (Koochesfahani & Dimotakis 1986). The imaged fluorescence represents the instantaneous product concentration, $C_P(y, \phi)$ at a given location (y) and a given stoichiometry (ϕ).

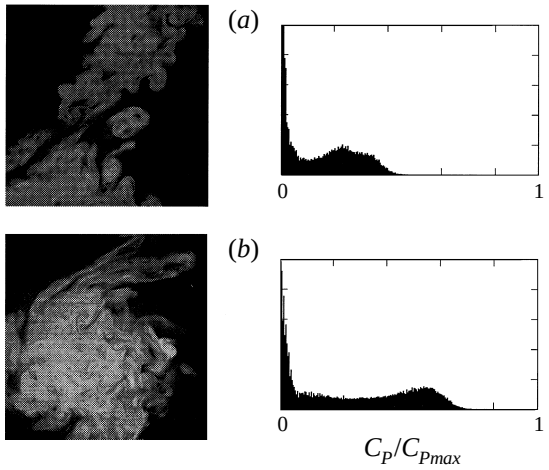

FIGURE 9. Chemical-reaction side views for the unstable $r = \frac{1}{4}$, $U_1 = 0.34$ m s^{-1} layer. (*a*) $\phi = 1/16$, (*b*) $\phi = 16$.

We next list the definitions of several quantities used for the data analysis; the reader is again referred to K & M for full details. The average chemical product concentration across the layer, which is obtained by averaging all images for each case, is given by

$$\theta_1(y) = \frac{\overline{C_P}(y, \phi \to \infty)}{C_{10}}, \quad \theta_2(y) = \frac{\overline{C_P}(y, \phi \to 0)}{C_{20}}.$$

The product thickness, δ_P, is defined as the total amount of product integrated across the entire layer. The normalized product thickness is defined as

$$\frac{\delta_{P_1}}{\delta} = \int_{-0.5}^{+0.5} \frac{\overline{C_P}(y, \phi \to \infty)}{C_{10}} \mathrm{d}(y/\delta),$$

and

$$\frac{\delta_{P_2}}{\delta} = \int_{-0.5}^{+0.5} \frac{\overline{C_P}(y, \phi \to 0)}{C_{20}} \mathrm{d}(y/\delta).$$

The cases examined using the chemical reaction technique (for both stable and unstable layers) are all the $r = \frac{1}{4}$ cases already examined using the passive scalar method. The magnification ratio employed was $m \approx 0.09$. The thickness of the layer was defined by the two points across the layer at which the average product concentration, $\overline{C_P}(y)$, had dropped to about 1 % of its peak value. All the thicknesses obtained were in excellent agreement with the ones obtained from the passive scalar data (see table 1). Accordingly, the values of Re and Rs/λ are the same as those quoted before.

Representative chemical-reaction images are presented in figure 9 (unstable) and in figure 10 (stable). In each of these figures, images (*a*) pertain to the $\phi = \frac{1}{16}$ reaction, and images (*b*) pertain to the $\phi = 16$ reaction. The fluorescence signal in these images now marks the chemical product formed. To the right of each image is the histogram for the $C_P/C_{P_{max}}$ values (the vertical axis is the probability). These images show that the maximum signal is never achieved anywhere in the layer, and that the signals for $\phi = 16$ are higher than for $\phi = \frac{1}{16}$; the latter observation already suggests that unequal entrainment characterizes the layer.

Based on images such as the ones just shown, various statistical quantities were evaluated. By averaging all the images, the average product-concentration distribution

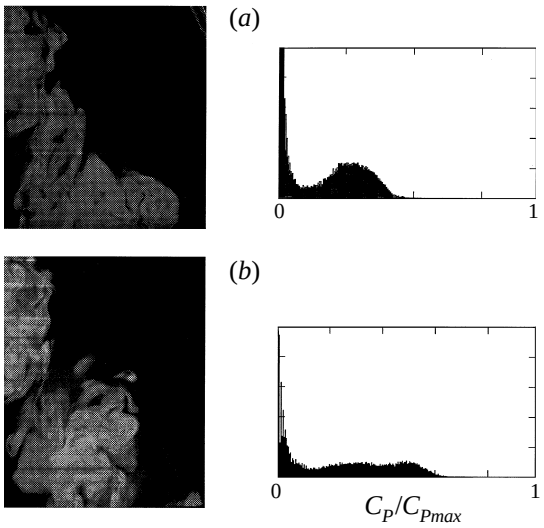

FIGURE 10. As figure 9 but for the stable layer.

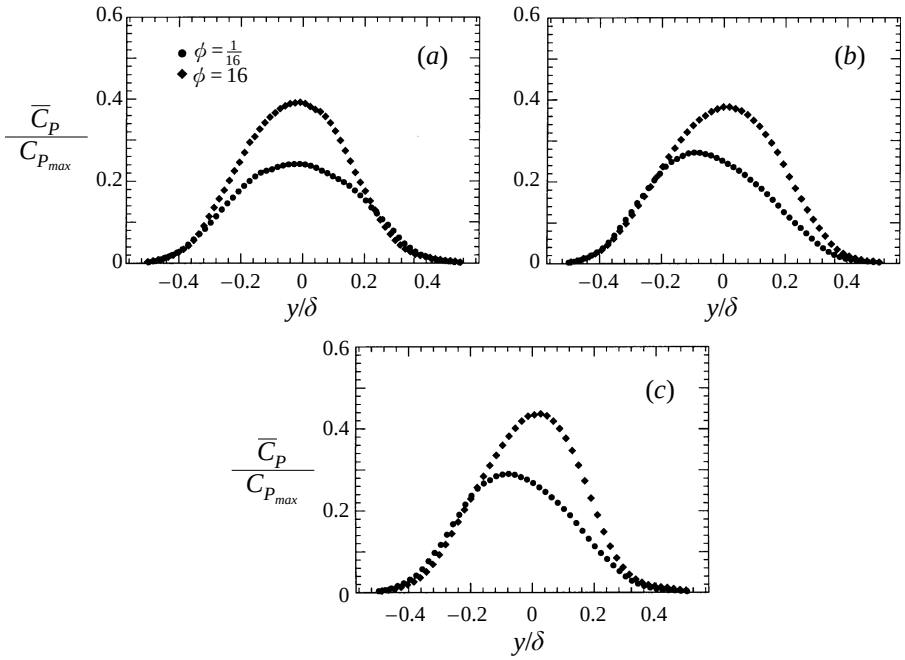

FIGURE 11. Average chemical-product profiles at $\phi = 16$ and $\phi = 1/16$, for the unstable layer. (*a*) $Rs/\lambda = 16.3$, (*b*) $Rs/\lambda = 27$, (*c*) $Rs/\lambda = 38.3$.

across the layer, $\overline{C_P}(y)/C_{P_{max}}$, was obtained for each case (and for each ϕ). The results are shown in figure 11 (unstable), and figure 12 (stable). For every case, it is seen that the $\phi = 16$ profile has a higher peak than the $\phi = \frac{1}{16}$ profile. As for the straight layers (K & M), flip experiments show that a different amount of product is formed when the same reactants are exchanged between the two free-stream sides. The present plots reveal that, for the least developed case ($r = \frac{1}{4}$, $U_1 = 0.34$ m s^{-1}) in both unstable (figure 11*a*, $Rs/\lambda = 16.3$) and stable (figure 12*a*, $Rs/\lambda = 17.8$) layers, the two flip profiles have

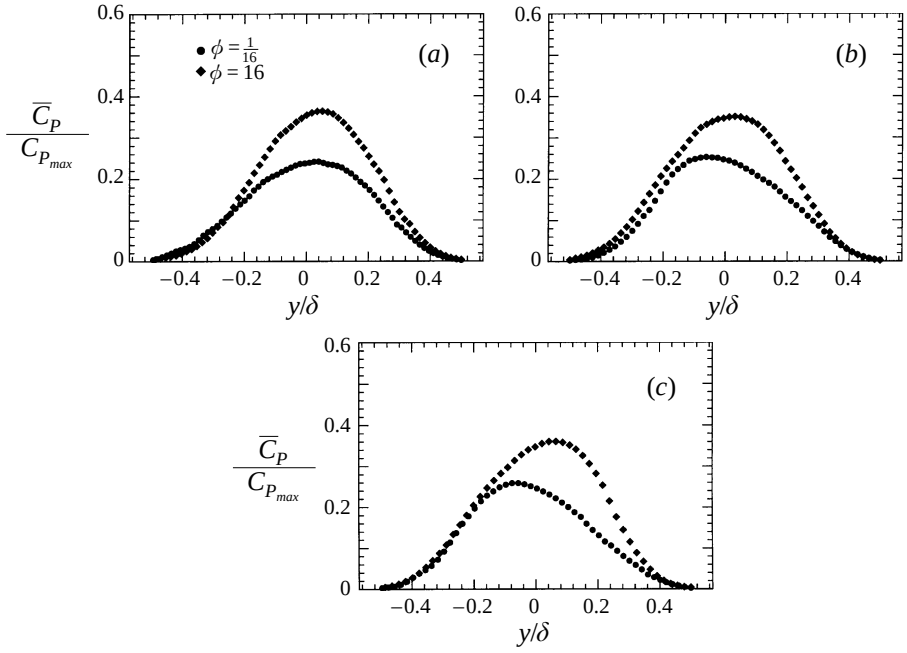

FIGURE 12. Average chemical product profiles at $\phi = 16$ and $\phi = 1/16$ for the stable layer. (*a*) $Rs/\lambda = 17.8$, (*b*) $Rs/\lambda = 29.5$, (*c*) $Rs/\lambda = 42$.

Rs/λ	$\frac{\delta_{P_1}(\phi = 16)}{\delta}$	$\frac{\delta_{P_2}(\phi = 1/16)}{\delta}$	C_M	E
16.3 (Unstable, $Re = 13600$)	0.169	0.122	0.581	1.39
17.8 (Stable, $Re = 13600$)	0.167	0.122	0.578	1.37
17.8 (Straight, $Re = 14000$)	0.171	0.125	0.578	1.37
27 (Unstable, $Re = 35000$)	0.178	0.128	0.582	1.39
29.5 (Stable, $Re = 33800$)	0.171	0.124	0.580	1.38
29.5 (Straight, $Re = 35000$)	0.174	0.128	0.576	1.36
38.3 (Unstable, $Re = 65000$)	0.181	0.130	0.582	1.39
42 (Stable, $Re = 63100$)	0.174	0.124	0.584	1.40
42 (Straight, $Re = 64000$)	0.179	0.132	0.576	1.36

TABLE 3. Chemical product and estimated mixed-fluid quantities, for curved and straight layers.

symmetric shapes with respect to $y = 0$. When the free-stream velocities are increased, and the layer becomes more fully developed, the flip profiles develop asymmetries (unstable: figure 11*b*, *c*; stable: figure 12*b*, *c*), where the peak of the mean product is tilted away from $y = 0$. This behaviour is identical to that of straight layers (at identical operating conditions respectively). The peak of the mean product is tilted towards the side of the layer carrying the lean reactant. The tilt in the curved layers is comparable to that in the straight cases, which is less than that in the gaseous-phase (straight) layers of Mungal & Dimotakis (1984). The absence of a tilt in figures 11(*a*) and 12(*a*) indicates that curved layers which are not fully developed have more homogeneous mixing across the layer.

The area under each $\overline{C_P}(y)/C_{P_{max}}$ profile gives the total amount of chemical product for the corresponding case. When this total amount of product is normalized by the

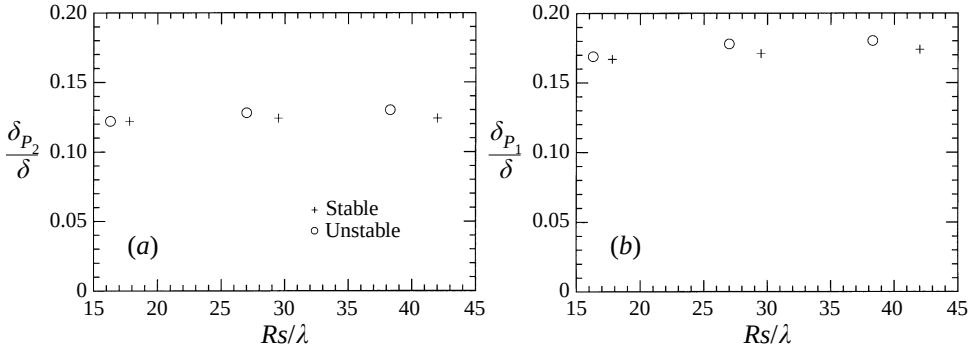

FIGURE 13. Normalized product thickness vs. Rs/λ for the curved layers: (*a*) low ϕ, (*b*) high ϕ.

layer's thickness, it yields, for each ϕ, the normalized product thickness (defined above), which is essentially the volume fraction of chemical product within the layer. The calculated product thicknesses are presented in table 3; they are also plotted as a function of Rs/λ in figure 13. Notice that in table 3 we also included the straight-layer results from K & M, for comparison.

The data show an increasing, albeit very slight, tendency of the mixing efficiency for both stable and unstable layers, as the pairing parameter is increased (the measured increases are within the measurement uncertainty). For the stable layer, the low-ϕ product thickness, δ_{P_2}/δ (low-ϕ), remains unchanged past the $Rs/\lambda = 29.5$ case, where δ_{P_1}/δ (high-ϕ) shows a continuous increase of about 2% within the range examined. The unstable layer has higher absolute values of the product thickness than the stable layer. Notice the increase ($\approx 5\%$) in both δ_{P_2}/δ and δ_{P_1}/δ when going from $Rs/\lambda =$ 16.3 to 27, but then a smaller increase of only $\approx 1.5\%$ when the pairing parameter is increased by the same amount (from $Rs/\lambda = 27$ to 38.3), suggestive of an asymptotic trend. This result suggests that the most developed unstable case measured is close to representing the fully developed regime.

4.1. *Estimates of mixed-fluid properties*

For each layer case, the pair of flip chemical-reaction data was used to make resolution-free estimates of several averaged mixed-fluid quantities within the layer. The probability $P_m(y)$ of finding mixed-fluid across the layer, is shown in figures 14(*a*) and 14(*b*) for the unstable and the stable layers respectively. The average mixed-fluid concentration distribution across the layer, $C_m(y)$, is shown in figure 15(*a*) for the unstable layers, and in figure 15(*b*) for the stable layers.

For the unstable layers, the $P_m(y)$ curves are similar for the first two cases, but the more fully developed $Rs/\lambda = 38.3$ shows an increase in the peak. Also notice that all three curves have their peaks at $y = 0$, whereas the maximum average signal was not necessarily symmetric around that value. The mixed-fluid distribution (figure 15*a*) shows a behaviour similar to the straight layers: the least developed case ($Rs/\lambda = 16.3$) is relatively flat across the layer (for $-0.3 \leqslant y/\delta \leqslant 0.3$), but the other two cases with a high pairing-parameter value develop a gradient. When fully developed, the layer shows a bias in the mixture fraction. In comparing these resolution-free estimates to the passive scalar results, it is remarkable to notice that the shift occurring in the shape of the $C_m(y)$ curves goes hand-in-hand with the PDF evolution (figure 7): a non-marching PDF corresponds to a flat $C_m(y)$ profile for the $Rs/\lambda = 16.3$ layer, but then both the PDF and $C_m(y)$ change for the two more fully developed layers.

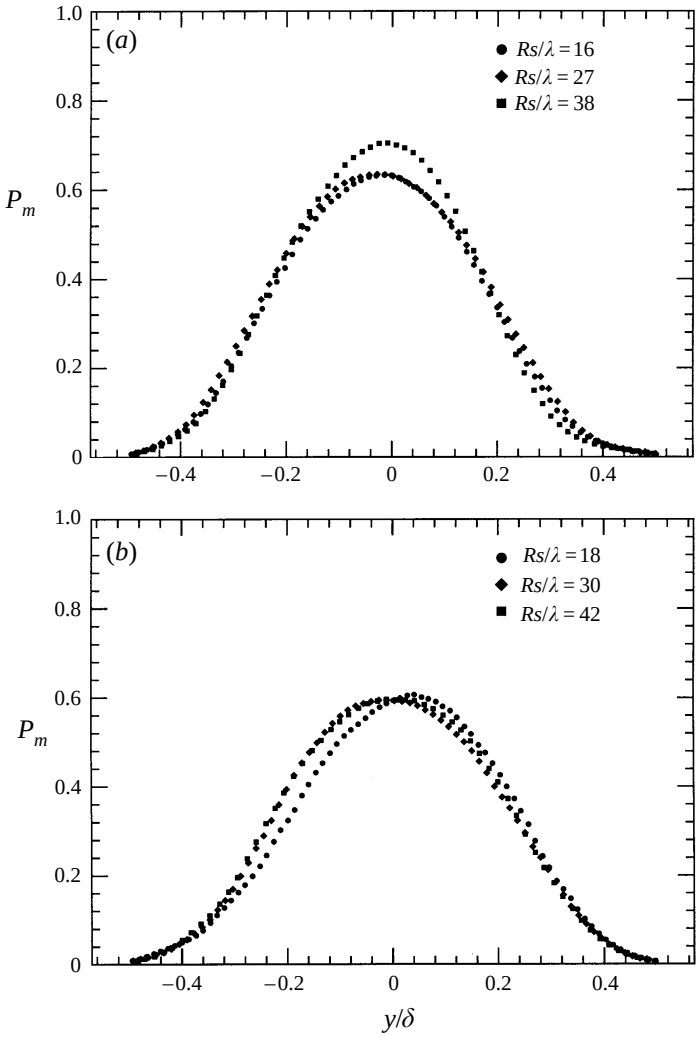

FIGURE 14. Mixed-fluid probability profiles for (*a*) the unstable layers, (*b*) the stable layers.

The stable layer has a mixed-fluid probability profile $P_m(y)$ which is practically identical for the three cases (figure 14*b*). The $C_m(y)$ profiles (figure 15*b*) are seen to gradually evolve for the three cases, with the least developed $Rs/\lambda = 17.8$ characterized as rather flat, the most developed $Rs/\lambda = 42$ showing a gradient similar to the straight and the unstable cases, and the middle case $Rs/\lambda = 29.5$ having a profile intermediate to these two cases. In relating these curves to the passive scalar PDF (figure 8), it is seen that the PDF changes smoothly from figures 8(*a*) to 8(*c*), with the non-marching portion gradually becoming marching.

Estimates for the total average mixed-fluid concentration C_M are given in table 3, along with estimates for the entrainment ratio, E. For both stable and unstable layers, the total average concentration shows a tendency for a slight increase when moving to a more developed turbulent regime. The composition ratio is in the 1.37 to 1.40 range, with the unstable layer having a constant value of 1.39. These values will be compared subsequently with the straight-layer values.

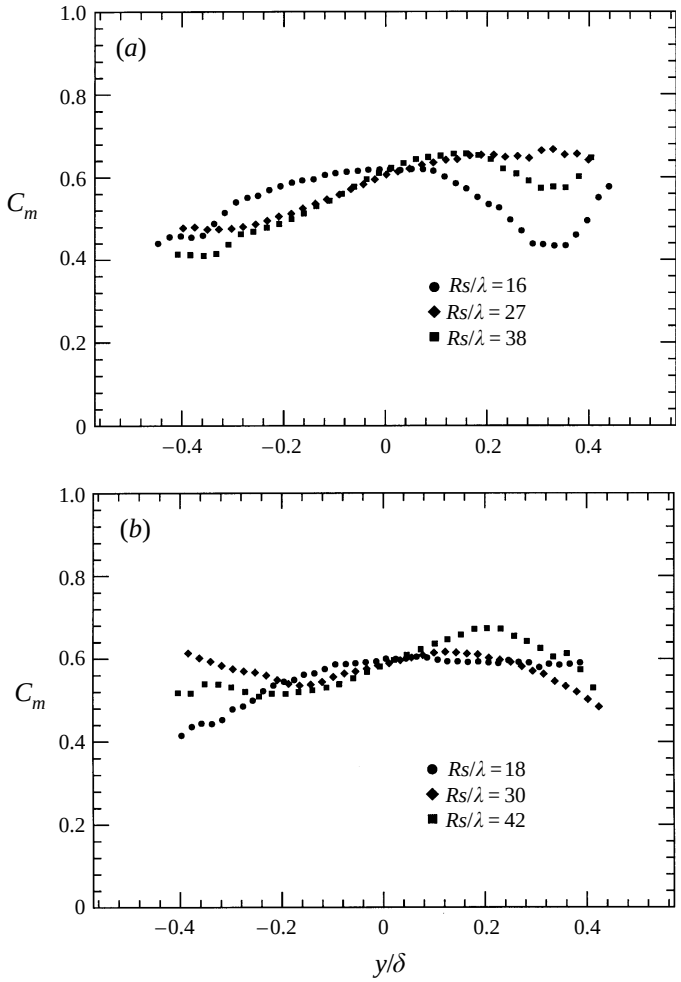

FIGURE 15. Averaged mixed-fluid composition profiles for (*a*) the unstable layers, (*b*) the stable layers.

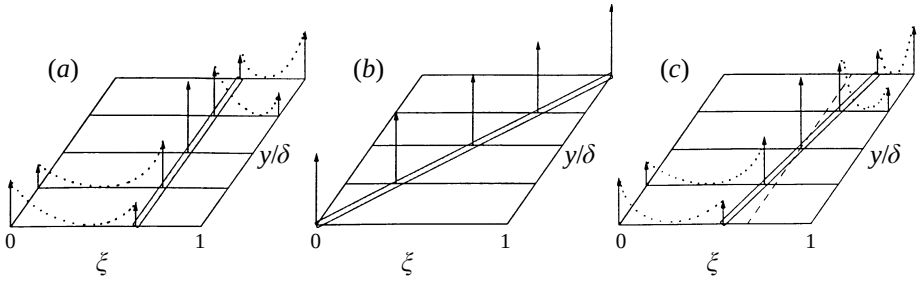

FIGURE 16. Idealized PDFs: (*a*) non-marching type, (*b*) marching type, (*c*) tilted type.

In summary, both unstable and stable layers evolve as they become more developed. Next, it would be interesting to establish a connection between the results obtained and the true (unmeasurable) mixture-fraction PDF of the curved layers. To facilitate our discussion in predicting the PDF, we reproduce in figure 16 idealized PDF-shapes, taken from K & M. We assume that the reader is familiar with the Broadwell–

Breidenthal (1982) model for mixing, which serves as the framework for the following analysis. At a regime just past the mixing transition (lowest Rs/λ), curved layers have mixed-fluid characteristics (figure 15) that correspond to a non-marching PDF (figure 16*a*). As the layer evolves, the $C_m(y)$ profiles develop a small bias towards each free-stream side (higher Rs/λ, figure 15). The measured change in the $C_m(y)$ distribution is small, and can be explained in two ways. (i) The PDF remains non-marching throughout the fully developed region (high Rs/λ-values), but the flame sheet (dotted lines in figure 16*a*), however small, increases its contribution, giving rise to the lateral variation in $C_m(y)$. (ii) The fully developed PDF is slightly tilted from edge to edge across the layer (figure 16*c*), while the flame sheet, which may or may not be evolving, has a negligible contribution. Here we remind the reader that, according to the Broadwell–Breidenthal model, the contribution of the flame sheet is expected to be almost negligible in high-Schmidt-number layers, which applies to the aqueous-phase layers ($Sc \approx 2000$) of this study.

4.2. *Comparisons with passive scalar results*

The same type of experiments as described in this work were previously performed for straight shear layers (K & M), and there we concluded that resolution limitations make passive scalar data unsuitable for quantitative estimates of mixing. Since the relative resolution in the present study is similar to that of straight layers, we expected (and actually found) a similar conclusion. A typical comparison between passive scalar and chemical reaction data is presented for just two cases. The amount of chemical product measured directly from the chemically reacting layers was compared to the PDF-based passive scalar predictions, for the stable $Rs/\lambda = 17.8$ case and the unstable $Rs/\lambda = 38.3$ case. The results appear in figure 17, where the severe overestimate of the amount of mixed fluid by the passive scalar techniques is obvious. With the exception of the stable $Rs/\lambda = 17.8$ case, figure 17(*a*), none of the passive scalar estimates showed any appreciable difference in the entrainment ratio, as each pair of 'calculated' flip profiles ($\phi = 16$ and $\frac{1}{16}$ curves) had similar (mirror-image) shape and height, as is demonstrated for the $Rs/\lambda = 38.3$ case, figure 17(*b*). The chemical reaction data, though, proved that there is a composition asymmetry in the mixed fluid for all cases. Other comparisons (not shown) and the similarity of the present results to K & M lead to the conclusion that the true PDF is of the tilted type and that the marching-type PDF in figure 16(*b*) is a poor predictor of all the results obtained from the (resolution-free) chemical reaction data.

Once more, it is clear that the passive scalar results are erroneous for quantitative predictions. However, whenever a change in the shape of the measured (passive scalar) PDF was observed, it was always accompanied by a true evolution in the scalar field, as depicted by the resolution-free chemical data for both curved layers (present work), and straight layers (K & M). Thus, passive scalar results, owing to their ease of performance, are of value in their ability to reflect qualitative flow changes, as seen in figures 7 and 8.

A final point deserving attention is the labelling of curved layers using the pairing parameter, Rs/λ. Following the findings in straight layers (K & M), it was decided that the Reynolds number is inadequate to characterize the structure of a shear layer. No detailed study of the hydrodynamic field for curved layers at various operating conditions exists (similar to the study of Huang & Ho 1990), but it is intuitively expected that curvature will act in such a way so as to make events happen either sooner or later in the Rs/λ-space. Unstable layers were seen to be more fully developed compared to stable layers at identical operating conditions. This result is consistent

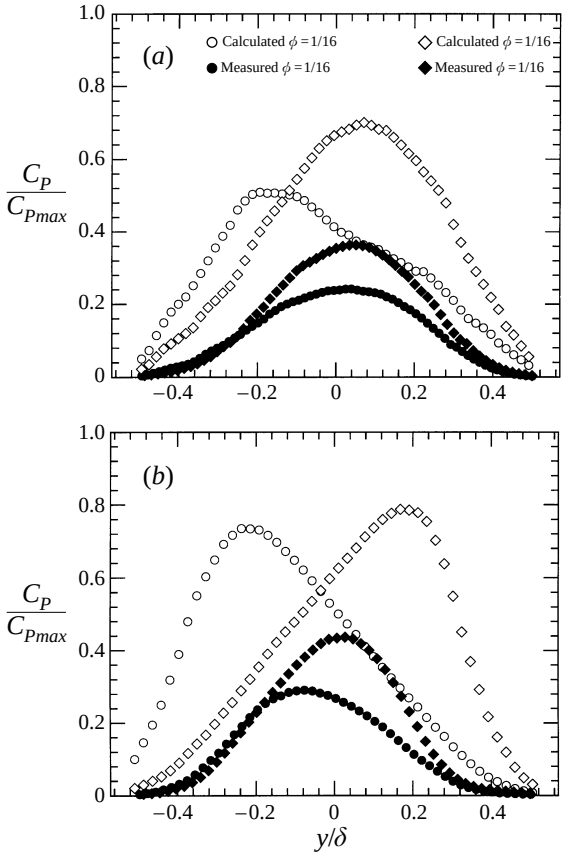

FIGURE 17. Comparison of measured and calculated (from the passive scalar PDF) average product concentration profiles for $\phi = 1/16$ and 16: (*a*) $Rs/\lambda = 17.8$ stable layer, (*b*) $Rs/\lambda = 38.3$ unstable layer.

with the hydrodynamic measurements of Plesniak & Johnston (1989). Hence, by virtue of the definition of the pairing parameter, unstable layers are expected to be more developed than stable ones, for the same pairing-parameter value. Thus, it is not inconsistent that for $U_1 = 0.34$ m s^{-1} ($r = \frac{1}{4}$), the unstable $Rs/\lambda = 16.3$ layer is more developed than its stable counterpart with $Rs/\lambda = 17.8$.

5. Comparisons with straight layers

We are now in a position to consider one of the questions which motivated studying curved mixing layers: does curvature produce mixing enhancement? The reader is reminded that unstable layers are documented in the literature to have larger growth rates (Wang 1984; present study), and also to have enhanced turbulent transport relative to the stable layer measured at identical conditions (Plesniak & Johnston 1989; Plesniak *et al.* 1994). Several conceivable ways thus exist for achieving mixing enhancement. The first is based on the fact that the unstable layer grows thicker, due to higher entrainment, and thus larger amounts of free-stream fluid are allowed to participate in the mixing process. A second possible mechanism for mixing enhancement (using an unstable configuration) is due to the enhanced turbulent

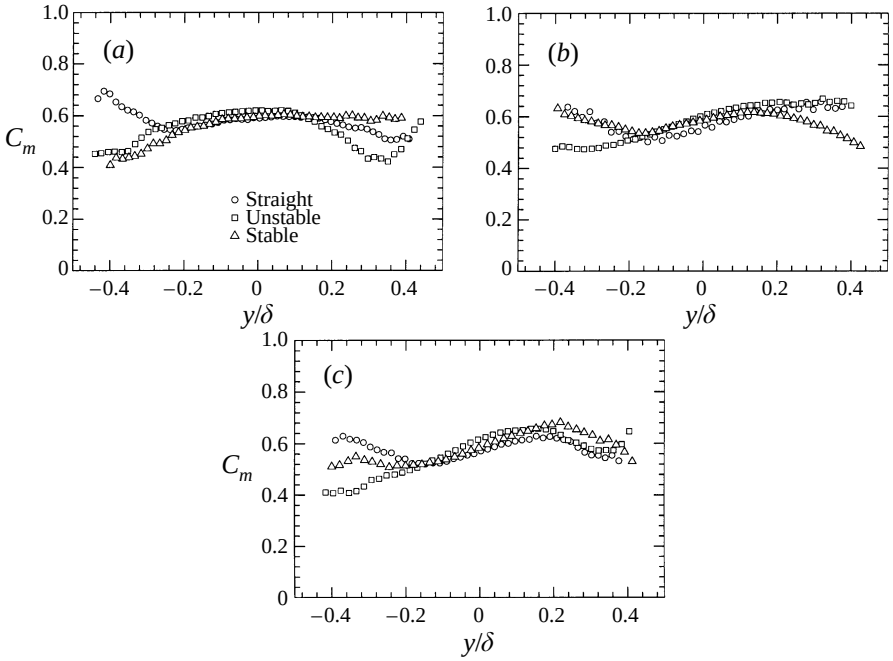

FIGURE 18. Comparison of average mixed-fluid composition for straight, unstable and stable layers: (*a*) $Rs/\lambda \approx 17$, (*b*) $Rs/\lambda \approx 29$, (*c*) $Rs/\lambda \approx 40$.

transport, with the smallest scales becoming more energetic and leading to better fine-scale mixing. Manifestations of mixing enhancement would be an increase in the probability of finding mixed fluid (at any mixture fraction) within the layer.

Comparisons for the mixed-fluid composition are shown in figure 18(*a–c*) for the three cases with $U_1 = 0.34$, 0.95 and 1.90 m s^{-1} ($r = \frac{1}{4}$) respectively. For each case, all three geometries have very similar shapes within the (more reliable) middle 50 % of the layer, suggesting that all layers have very similar scalar structure. In the non-fully developed state (figure 18*a*), all liquid layers have a uniform profile across the layer. When the layer is pushed to a more developed state, the mixed-fluid composition develops a lateral variation (gradient) across the layer (figure 18*b*). Subsequently, a similar gradient characterizes all three layers when the operating conditions are further pushed (figure 18*c*) (the Reynolds number for the cases in figure 18*c* is about twice that of figure 18*b*). This suggests that the curves in figure 18(*c*) may be representative of the asymptotic behaviour in liquid layers. For all (liquid) layers, this asymptotic behaviour is different than the gaseous-phase layer of Mungal (see Koochesfahani & Dimotakis 1986), which reflects the fact that molecular diffusion remains important in all turbulent regimes. Also, for all three sets of operating conditions, the unstable layers ($-0.25 \leqslant y/\delta \leqslant 0.05$) show mixed-fluid compositions which are 4–5 % higher than those of the straight layers (stable layers lie between unstable and straight). Finally, we note that the results of all three geometries give credence to the Broadwell–Breidenthal model, in predicting that in a liquid layer molecular mixing is quite insensitive to an increase in the Reynolds number.

The mixed-fluid probability distributions, P_m, for all three geometries are shown in figure 19. For the first two operating conditions, figure 19(*a*, *b*), all three layers have essentially the same profiles. In the most fully developed case, the stable layer has a lower peak value, suggesting that the straight and unstable layers are slightly better

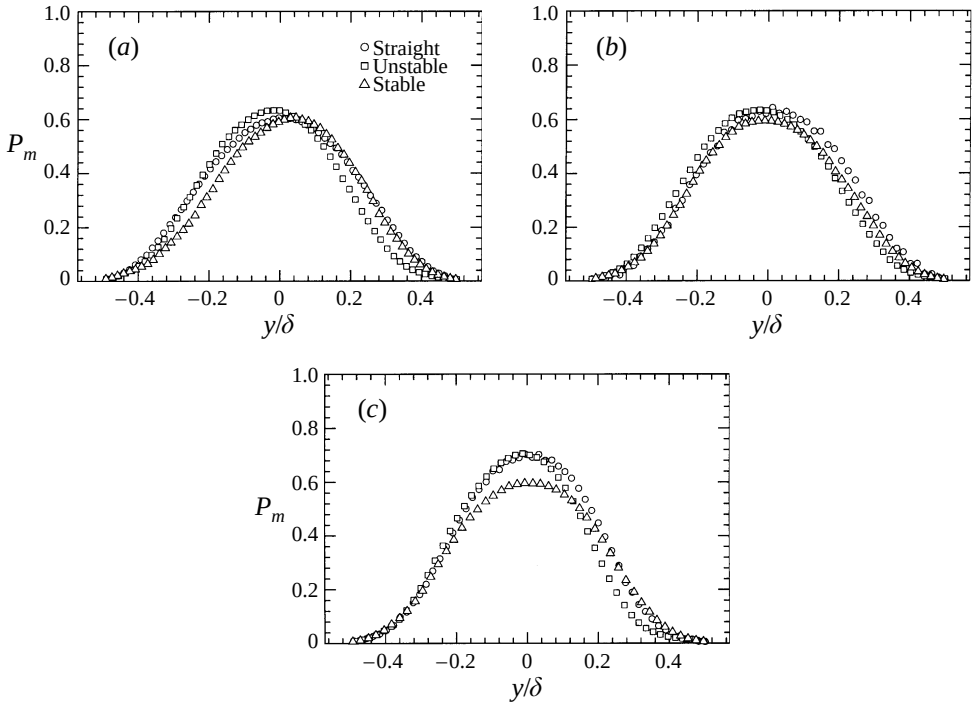

FIGURE 19. Comparison of mixed-fluid probability for straight, unstable and stable layers: (*a*) $Rs/\lambda \approx 17$, (*b*) $Rs/\lambda \approx 29$, (*c*) $Rs/\lambda \approx 40$.

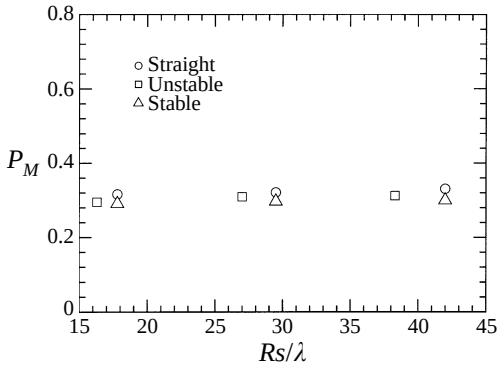

FIGURE 20. Comparison of total mixed-fluid probability among straight, unstable, and stable layers.

mixers, but the change is not large. A comparison of the total (normalized) mixed-fluid probability, P_M, is shown in figure 20. Recall that P_M is the integral under each of the $P_m(y)$ profiles (figure 19); the quantity P_M essentially represents the total volume fraction of mixed fluid (at any composition) within the layer. The volume fraction of mixed fluid is seen to remain unchanged for all three geometries. With respect to the unstable layer in particular, it is seen that the structural changes observed in the hydrodynamic field (Plesniak *et al.* 1994) do not lead to a larger amount of mixed fluid. From an engineering point of view, this result is important because, once the layer

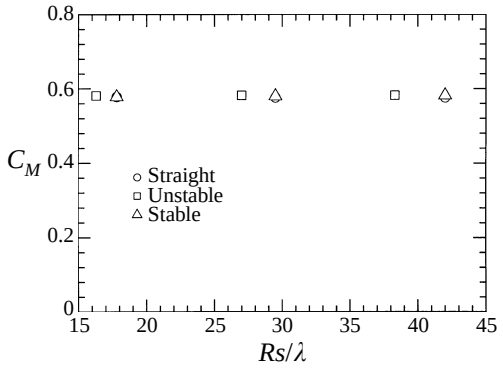

FIGURE 21. Comparison of total mixed-fluid average composition among straight, unstable, and stable layers.

thickness δ is known, the estimated mixed-fluid thickness for all (curved and straight) liquid layers is $\approx 0.30\delta$.

Figure 21 shows the average composition of the mixed fluid in the layer, C_M, which was estimated based on the flip chemical-reaction experiments. This plot shows another surprising result: beyond the mixing transition, C_M remains constant at ≈ 0.58 for all liquid-layer geometries. Koochesfahani & Dimotakis (1986) first conjectured that C_M was constant for straight liquid layers (past the mixing transition). The present study has shown that the straight layer continues to change past the conditions examined by Koochesfahani & Dimotakis (1986), and in its asymptotic state shows a small lateral variation of the mixed-fluid concentration, $C_m(y)$. Despite this change, the (integrated) quantity C_M remains unchanged. The present results become even more surprising when unstable layers are considered. Flow visualizations by Wang (1984) and detailed velocity measurements by Plesniak *et al.* (1994) had shown evidence of enhanced turbulent transport and three-dimensionality for the unstable layer. In terms of scalar mixing, no observable changes in the mixing efficiency are measured. This character of scalar mixing, as depicted in figures 20 and 21, deserves attention, since it demonstrates that the enhancement of streamwise vorticity may alter the extent of the layer (and possibly the location of the mixing transition), but little is done to change the mixedness: both the composition and the volume fraction of mixed fluid are practically the same for all three geometries. We should now consider these findings in the context of the corresponding velocity measurements.

6. Relation to hydrodynamic measurements

A detailed comparison of the velocity fields among straight, stable and unstable shear layers, was recently performed by Plesniak *et al.* (1994), who expanded on the original work by Plesniak & Johnston (1989) to study the effects of stabilizing and destabilizing curvature on the hydrodynamic structure of the layer. They concluded that for both stable and unstable layers, streamwise vortical structures are the result of amplification of incoming disturbances (as in a straight layer), and not of the Taylor–Görtler instability. The (untripped) unstable layer was found to have a vorticity thickness about 15% higher than the corresponding straight layer, and about 40% higher than the stable layer. The peak of the mean streamwise vorticity was highest for unstable layers (with straight following, and stable having the lowest value),

resulting in significant spanwise variation (and intermittency). In the far field, the peak of the primary Reynolds stress was measured to be 66% higher for the unstable layer than for the stable layer, while the turbulent kinetic energy was 44% larger. The velocity spectra also showed significant differences between unstable and stable layers.

It is challenging to explain why the enhancement of momentum mixing does not lead to increased scalar mixedness. A first issue which must be kept in mind is the difference between the momentum-diffusion and the scalar-diffusion scales, which for the present liquid-phase layer is significant. The study of Plesniak *et al.* (1994) showed that the entire range of turbulent scales (from the largest to the dissipative) are more energetic for the unstable layer than for the stable layer at identical conditions. Larger scales contribute to the engulfment of irrotational fluid, and to the entrainment by the large-scale structures. The present study confirmed that the unstable layer entrains more fluid, and thus grows thicker. However, larger scales do not directly contribute to mixing at a molecular level. A first question then is whether increased energy in the range of scales from δ (largest) to scales which are small, but bigger than the scalar dissipation length, necessarily leads to better fine-scale mixing. The answer may not be unique; the present measurements tend to show a decoupling between the stirring and the mixing process: it appears that the stirring process is such that the volume fraction of fluid over which scalar dissipation takes effect is the same for all geometrical configurations. The unstable layer was also found to be (hydrodynamically) more intermittent than the stable layer; notice however, that lack of scalar fluctuations is an indication of better homogenization. Finally, increasing the turbulence intensity in regions of the flow where two fluid elements are already molecularly mixed may not result in any mixing enhancement within that region. As an analogy, imagine a container in which two distinct fluids are placed. By the action of a stirrer the two fluids can be mixed, after a certain time (or space). Additional stirring will not produce any more measurable mixing.

Since more fluid is entrained in the unstable layer due to the enhanced activity of large scales, it follows that the smallest scales adjust in order to keep the volume fraction of molecularly mixed fluid the same as in the straight and stable layers. It thus appears that in liquid turbulent shear flows, the rate of scalar dissipation scales directly with the large-scale entrainment rate, despite the differences in the velocity spectra for the various geometries. It is also conceivable (as pointed out by Professor S. Lele, private communication) that the hydrodynamic data could be normalized appropriately so that spectra of both stable and unstable layers would collapse onto each other. The normalizing parameters could then be used, through a transport equation, to show that the enhanced turbulent transport scales exactly with the enhanced growth rates in unstable layers. As a final word of caution, the far-field measurements of Plesniak *et al.* (1994) were performed at a downstream distance where the layer's thickness was large enough for test-section confinement effects to be significant, as shown by Wood & Bradshaw (1982).

7. Comparison with layers of unequal density

We now make some comparisons between the present curved layers and the unequal-density gaseous-phase straight mixing layer of Frieler & Dimotakis (1988). Although the two cases seem quite different, interesting analogies may be drawn about the nature of shear-layer flows. The motivation for this comparison is that the present measurements have shown that the mixedness remains the same, independent of the effects of curvature. The enhanced turbulence transport in the shear region was

accompanied only by a change in the net growth rate of the layer. The scalar mixing efficiency proved to be insensitive to all the reported effects of curvature on the velocity field.

Frieler & Dimotakis (1988) performed chemical-reaction experiments in gaseous layers for various density ratios $s = \rho_2/\rho_1$, ranging from 4 to $\frac{1}{7}$. Their results showed differences in the total average mixed-fluid composition, C_M, for the various values of s. However, the total volume-fraction (probability) of mixed fluid within the layer, P_M, was insensitive to the free-stream density differences. Additionally, the distribution of mixed fluid across the layer, $P_m(y)$, was relatively insensitive to the changes in density ratio. This result is quite remarkable, and analogous to the insensitivity of the present study's layers to the effects of curvature. Wang's flow visualizations have shown significant changes in the layer when the heavier and the lighter fluid are interchanged in the two free-stream sides. By analogy with the effects of curvature, a Rayleigh–Taylor instability is known to develop in unequal-density layers, depending on the placement of the two fluids, giving rise to a stable and a unstable case. The (unstable) Rayleigh–Taylor instability is seen in Wang's images to produce significant enhancement in the growth rate, and loss of coherent structures (the latter must be considered with caution, since these are shadowgraphs).

We thus have two different shear layers (the curved layers of this study, and the non-homogeneous layer of Frieler & Dimotakis) where mechanisms which produce changes in the growth rate (and also have other effects) have a negligible effect on the percentage of total mixed fluid into the layer. This observation is significant for our understanding of turbulent mixing. The steps leading to molecular mixing appear to be very robust in shear layers, unaffected by the enhancement of certain instabilities. Experiments in forced mixing layers could shed more light in that direction, and are discussed next.

8. Relation to forced layers

Roberts (1985) performed experiments in forced, aqueous-phase, straight mixing layers to measure the growth rate and the amount of chemical product formed under different forcing frequencies. Most of his results are at low Reynolds numbers, where the effects of forcing cannot be isolated from mixing-transition effects. However, experiments were run at conditions identical to those of Koochesfahani & Dimotakis ($r = 1/2.63$, $U_1 = 0.70$ m s^{-1}), and measurements obtained up to a downstream distance of $x \approx 24$ cm; Koochesfahani & Dimotakis (1986) measured their layer at $x = 25$ cm where $Re = 23\,000$, and hence Roberts' post-mixing-transition layers are not yet fully developed (K & M). For the unforced layer, Roberts essentially duplicated the results of Koochesfahani & Dimotakis: the layer grows linearly with downstream distance, and, past the mixing transition, the amount of product, δ_P, grows in exact proportion to the layer's width; thus, the normalized product thickness, δ_P/δ, is fixed past the mixing transition. When the same layer was forced at a frequency of $F = 8$ Hz (the initial most unstable frequency of the layer was $F_0 \approx 63$ Hz), it developed a region of no growth (locked-in structures), suggesting that the layer has ceased entraining fresh free-stream fluid. Within this flat region, the amount of product (δ_P) remained unchanged. This finding is intriguing considering that, although the layer does not grow in that flat region, the layer's structures continue to roll (the layer has not come to rest!). Despite this turbulent action, no additional molecularly mixed fluid is produced. This result, again, bears an analogy to the present study's unstable layer, where additional turbulent transport (with respect to the straight layer) did not result

in an enhancement of the volume fraction of mixed fluid (in our case the layer continuously entrains fresh fluid).

We also note that Koochesfahani & MacKinnon (1991) used the passive scalar technique to investigate the effects of forcing upon a shear layer at mixing-transition conditions and also report a similar increase in the total amount of mixed fluid associated with the enhanced spreading, but with little change in small-scale mixing. Thus, forcing again does not appear to be able to change the mixing efficiency.

9. Conclusions

Experiments were performed in liquid shear layers using mild stabilizing and destabilizing curvature. In the fully developed regime, the unstable layer was seen to have higher growth rate than the straight and the stable layers. The mixing characteristics of both unstable and stable layers follow closely those of the straight layer. At conditions past the mixing transition, but not representative of the far field, both stable ($Rs/\lambda = 16.3$) and unstable ($Rs/\lambda = 17.8$) layers show symmetric chemical product profiles in flip experiments. The estimated (based on the chemical product data) mixed-fluid composition is uniform across the layer. At more fully developed conditions, the flip product profiles develop asymmetries. Accordingly, the estimated mixed-fluid composition develops a small lateral variation; this variation was always smaller than that seen in straight gaseous-phase layers. As was found for the straight layer, the chemical data indicate that the fully developed PDF for curved liquid layers is likely to be of the tilted type, with the marching PDF being a poor representation.

Both unstable and stable reacting layers produced small increases in the amount of product as the pairing parameter increased (or as the Reynolds number increased at a fixed speed ratio). The amount of mixed fluid (and of chemical product formed) was larger for the unstable layers examined, but always in fixed proportion to the layer's thickness. Thus increased stirring leads to a proportional increase in mixing, but mixing efficiency is unchanged. Very interesting conclusions result from comparing straight to curved layers. For each of the operating conditions examined, all three geometries have a very similar mixing efficiency. Both the total mixed-fluid composition, and the total probability of mixed-fluid into the layer were practically the same for unstable, straight, and stable layers. This finding is intriguing, since hydrodynamic measurements have shown that the energy content of unstable layers is greater than that of straight or stable layers. In conclusion, for all liquid shear layers the rate of scalar mixing is directly proportional to the layer's growth rate (which is a marker of the entrainment rate), and not to any hydrodynamic measures.

The authors wish to thank Professor P. Bradshaw for helpful discussions. The financial support of the NASA/Stanford Center for Turbulence Research and of the National Science Foundation (grant number CTS-9020641) is greatly appreciated.

REFERENCES

Bell, J. H. & Mehta, R. D. 1990 Development of a two-stream mixing layer from tripped and untripped boundary layers. *AIAA J.* **28**, 2034.

Bradshaw, P. 1973 Effects of streamline curvature on turbulent flow. *AGARD-AG*-169.

Broadwell, J. E. & Breidenthal, R. E. 1982 A simple model of mixing and chemical reaction in a turbulent mixing layer. *J. Fluid Mech.* **125**, 397.

Frieler, C. E. & Dimotakis, P. E. 1988 Mixing and reaction at low heat release in the non-homogeneous shear layer. *AIAA Paper* 88-3626.

GIBSON, M. M. & YOUNIS, B. A. 1983 Turbulence measurements in a developing mixing layer with mild destabilizing curvature. *Exps. Fluids* **1**, 23.

HUANG, L.-S. & HO, C.-M. 1990 Small scale transition in a plane mixing layer. *J. Fluid Mech.* **210**, 475.

JIMENEZ, J. 1983 A spanwise structure in the plane shear layer. *J. Fluid Mech.* **132**, 329.

KARASSO, P. S. 1994 Experiments on mixing and reaction in plane and curved shear layers. PhD thesis, Stanford University.

KARASSO, P. S. & MUNGAL, M. G. 1996 Scalar mixing and reaction in plane liquid shear layers. *J. Fluid Mech.* **323**, 23 (referred to herein as K & M).

KOOCHESFAHANI, M. M. & DIMOTAKIS, P. E. 1986 Mixing and chemical reactions in a turbulent liquid mixing layer. *J. Fluid Mech.* **170**, 83.

KOOCHESFAHANI, M. M. & MACKINNON, C. G. 1991 Influence of forcing on the composition of mixed fluid in a two-stream shear layer. *Phys. Fluids* A **3**, 1135.

LIOU, W. W. 1993 Linear instability of curved free shear layers. *NASA Tech. Mem.* 106290.

MARGOLIS, D. P. & LUMLEY, J. L. 1965 Curved turbulent mixing layer. *Phys. Fluids* **8**, 1775.

MUNGAL, M. G. & DIMOTAKIS, P. E. 1984 Mixing and combustion with low heat release in a turbulent mixing layer. *J. Fluid Mech.* **148**, 349.

PLESNIAK, M. W. & JOHNSTON, J. P. 1989 The effects of longitudinal curvature on turbulent two-stream mixing layers. *Mech. Engng Dept Rep.* MD-54. Stanford University.

PLESNIAK, M. W., MEHTA, R. D. & JOHNSTON, J. P. 1994 Curved two-stream turbulent mixing layers: three-dimensional structure and streamwise evolution. *J. Fluid Mech.* **270**, 1.

RAYLEIGH, LORD 1880 On the stability, or instability, of certain fluid motions. *Proc. Lond. Math. Soc.* **11**, 57.

ROBERTS, F. A. 1985 Effects of a periodic disturbance on structure and mixing in turbulent shear layers and wakes. PhD thesis, Caltech.

SYNGE, J. L. 1933 The stability of heterogeneous liquids. *Trans. R. Soc. Canada* **27**, 417.

WANG, C. 1984 The effects of curvature on turbulent mixing layers. PhD thesis, Caltech.

WOOD, D. H. & BRADSHAW, P. 1982 A turbulent mixing layer constrained by a solid surface. Part 1. Measurements before reaching the surface. *J. Fluid Mech.* **122**, 57.

WYNGAARD, J. C., TENNEKES, H., LUMLEY, J. L. & MARGOLIS, D. P. 1968 Structure of turbulence in a curved mixing layer. *Phys. Fluids* **11**, 1251.